Chemistry–A European Journal

Research Article
doi.org/10.1002/chem.202202891

Chemistry Europe
European Chemical Societies Publishing

www.chemeurj.org

Promoted Photothermal Catalytic CO Hydrogenation by Using TiC-Supported Co–Fe_5C_2 Catalysts

Special Collection

Haoyang Jiang[+],[a] Feng Zhu[+],[a] Renjie Zhou,[a] Linyu Wang,[a] Yongcheng Xiao,[a] and Miao Zhong*[a]

Abstract: Photothermal catalytic CO hydrogenation offers the potential to synthesize light hydrocarbons by using solar energy. However, the selectivity and activity of the reaction are still far below those achieved in conventional thermal catalytic processes. Herein, we report that the Co-modified Fe_5C_2 on TiC catalyst promotes photothermal catalytic CO hydrogenation with a 59% C_{2+} selectivity in the produced hydrocarbons and a 30% single-pass CO conversion at a high gas hourly space–time velocity of 12000 mL g^{-1} h^{-1}. Using in-situ-irradiated XPS, we show that light-induced hot electron injection from TiC to Fe_5C_2 modulates the chemical state of Fe, thereby increasing the CO-to-C_{2+} conversion. This work suggests that it is possible for plasmon-mediated surface chemistry to enhance the activity and selectivity of photothermal catalytic reactions.

Introduction

Fischer-Tropsch Synthesis (FTS) is a widely adopted industrial process to synthesize valuable hydrocarbons and oxygenates from syngas ($CO/H_2 = 0.5–3$) at 150–300 °C, 5–50 atm.[1] In the traditional thermal catalytic FTS process, a large amount of fossil-fuel energy is consumed, resulting in massive CO_2 emissions. Following the Anderson-Schulz-Flory distribution,[2] the thermal catalytic FTS produces a wide range of hydrocarbons, and the selectivity to the important C_2–C_3 alkanes remains poor.

Photothermal catalysis which uses photon energy to heat the catalyst surfaces and drive the chemical reactions[3–5] is an alternative route to offset the strong reliance on fossil fuels. Recently, solar-driven CO_2/CO photoreduction[6–9] and renewable-powered CO_2/CO electrolysis[10–12] have been intensively studied. In the photo-driven reactions, besides the photo-to-thermal energy conversion, the light-induced plasmonic hot-electron injection has been reported[13–15] to improve the reaction activity and selectivity.[16] Guo et al.[17] reported a graphene-supported Ru catalyst catalyzed FTS at mild conditions (150 °C, 2.0 MPa H_2, and 1.0 MPa CO) under visible-light irradiation and achieved a high catalytic activity and high C_{5+} selectivity. They suggested that the excited electrons in Ru were injected into the antibonding states of CO molecules to enhance CO dissociation. Zhang et al.[18] reported a series of MnO-supported Ni catalysts that showed high photothermal catalytic CO hydrogenation performance with a C_2–C_4 selectivity of 33% under ultraviolet-visible irradiation. They used X-ray photoelectron spectroscopy (XPS) and X-ray absorption spectroscopy (XAS) to show that electron transfer from MnO to Ni nanoparticles modified the electronic structure of Ni to favor CO hydrogenation toward light olefins. He et al.[19] reported that cobalt plasmonic superstructures with inter- and intra-band transition absorption enhanced plasmonic excitation and improved photothermal CO_2 hydrogenation. These reports indicated that a synergy between the photothermal effect and plasmonic behavior is possible to improve the reaction kinetics and catalytic activity.

To broaden the light absorption into the full solar spectrum, metal carbides such as TiC and Mo_2C are promising candidates with wide plasmonic absorption wavelengths. Combining plasmonic metal carbides and active FTS catalysts is therefore expected to improve photothermal catalytic activity. Among the thermal FTS catalysts, Co- and Fe-based catalysts have been widely studied because they are active for C–C coupling and C–H bond formation with long reaction durability.[20] Zhang et al.[21] reported Co catalysts derived from layered-double-hydroxide nanosheets for improved photothermal CO-to-ethanol conversion with a C_{2+} hydrocarbon selectivity of 65.0% and a CO conversion of 35.4%. Ma et al.[22] synthesized Fe_5C_2 nanoparticles showing enhanced CO conversion and improved C_{5+} selectivity compared to the conventional reduced-hematite catalysts. Gevert et al.[23] showed that Co incorporated Fe_2O_3 increased the reducibility of Fe in Fe–Co/γ-Al_2O_3 catalysts and enhanced CO hydrogenation.

In this work, we synthesized Co-doped Fe_5C_2 catalysts on TiC supports exhibiting excellent photothermal catalytic CO hydrogenation performance to produce C_{2+} chemicals. TiC absorbs light up to 2500 nm, thereby heating the catalyst

[a] Dr. H. Jiang,[+] F. Zhu,[+] R. Zhou, L. Wang, Y. Xiao, Prof. Dr. M. Zhong
College of Engineering and Applied Sciences
National Laboratory of Solid State Microstructures
Jiangsu Key Laboratory of Artificial Functional Materials
Nanjing University
163 Xianlin Avenue, Qixia District, Nanjing 210023 (P. R. China)
E-mail: miaozhong@nju.edu.cn

[+] These authors contributed equally to this work.

Supporting information for this article is available on the WWW under https://doi.org/10.1002/chem.202202891

Special Collection This manuscript is part of a Special Collection "Brightening the Future with Photocatalysis".

surfaces. Fe_5C_2 was formed in situ on TiC during photothermal catalytic CO hydrogenation. Adding Co into Fe_5C_2/TiC further enhanced the CO conversion compared to the pristine Fe_5C_2/TiC likely because that Co functioned as an H_2-dissociation promoter. In situ irradiated XPS showed that the light-induced hot electron injection from TiC to Co–Fe_5C_2 likely modulated the chemical states of Fe to improve the photothermal catalytic activity. We obtained a 59% C_{2+} selectivity in the produced hydrocarbons and a 30% single-pass CO conversion at a high gas hourly space-time velocity of 12000 mL g^{-1} h^{-1}. The selectivity of C_2–C_3 hydrocarbons increased 1.5 times compared to that of the same Co–Fe_5C_2/TiC catalysts under thermal catalytic conditions without light illumination. Through a comparative experiment, we showed that the photothermal catalytic CO hydrogenation activity was drastically decreased by more than half using the same Co–Fe_5C_2/TiC catalysts after coating a thin surface layer of TaC. The thin TaC layer transported photothermal heat to the underlayer Co–Fe_5C_2/TiC to enable an identical surface temperature as that of Co–Fe_5C_2/TiC under illumination. TaC also blocked light illumination on Co–Fe_5C_2/TiC catalysts to eliminate plasmonic hot electron generation. The reduced performance with TaC-coated Co–Fe_5C_2/TiC indicated that both the photo-to-thermal effect and plasmonic hot electron injection contributed to CO hydrogenation in the case using Co–Fe_5C_2/TiC catalysts. This work suggests that plasmon-mediated surface chemistry could improve the activity and selectivity in photothermal catalysis.

Results and Discussion

The schematic of the photothermal catalytic CO hydrogenation on Co–Fe_5C_2/TiC catalysts is shown in Figure 1. TiC, Co/TiC, Fe/TiC, and Co–Fe_5C_2/TiC all exhibit broadband light absorption across the visible-to-near-infrared spectrum with an absorption rate of 90–97% in Figure S1 in the Supporting Information. As indicated in the previous studies,[24–27] TiC is a broadband light absorber and plasmonic material with strong localized surface plasmon resonance (LSPR) absorption in the near-infrared region. Therefore, a portion of the incident light is absorbed by TiC and is converted to surface heat for the CO hydrogeneration reaction by a photo-to-thermal contribution. In addition, owing to the favorable electronic energies (Fermi levels) between Ti^0 in TiC and Fe/Fe^{2+} in Fe_5C_2, light-induced hot electrons can transfer from TiC to the adjacent Fe_5C_2 to reduce the chemical states of Fe from +2 to +(2-σ). As reported,[28] the reduced and electron-rich Fe sites are more active for H_2 dissociation and C–H bond formation. The CO hydrogeneration activity is therefore expected to be further improved through a plasmonic contribution.

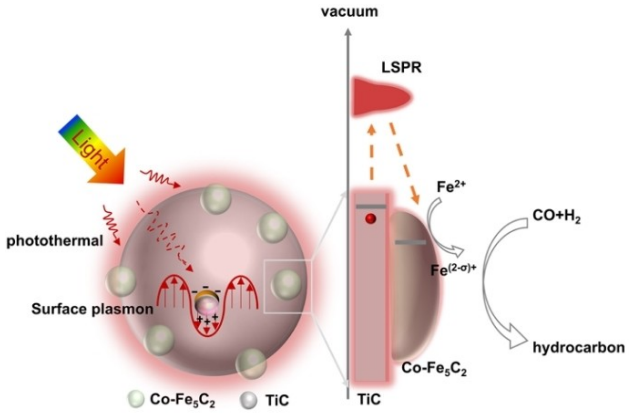

Figure 1. Schematic of the photothermal catalytic CO hydrogenation on the TiC-supported Co–Fe_5C_2 catalysts.

To synthesize the catalysts, we loaded Fe and Co onto the surfaces of TiC nanopowders by wetness impregnation with a fixed Metal/TiC proportion of 15 wt%. As a common strategy, we impregnated K_2CO_3 precursor to introduce K^+ promoters for hydrocarbon formation. The Fe- and Co-loaded catalysts were denoted Co/TiC and Fe/TiC, respectively. The Fe and Co co-loaded catalysts with different Fe/Co mass ratios of 5:1 and 2:1 were denoted Fe–Co(5:1)/TiC and Fe–Co(2:1)/TiC, respectively. The carburization of the initially loaded Fe to Fe_5C_2 was obtained in situ in CO gas flow during the photothermal catalytic reaction. Figure 2a and b show the X-ray diffraction (XRD) patterns of the catalysts before and after the reaction. The distinct diffraction peaks at 35.6°, 41.4°, and 60.2°, assigned to the (111), (200), and (220) faces of fcc-structured TiC, were observed in all the samples before and after the reaction. It indicated that TiC did not undergo a phase transition or oxidation during the reaction. As for the Fe content in the catalysts before reaction, intensive signals were observed at ~44.5°, which were assigned to the (110) face of α-Fe. Compared to Fe/TiC, the positions of α-Fe (110) in Fe–Co/TiC shifted from 44.3° to 44.7°, likely because the alloying Co atoms in α-Fe reduced the lattice constant. No obvious peaks of metallic Co or Co-related oxides were found in the Fe–Co/TiC samples. As shown in Figure 2b, the diffraction peaks of α-Fe in Fe/TiC and Fe–Co/TiC disappeared after the reaction. The appearance of new peaks at 43.4° and 44.1° were assigned to the (021) and (510) faces of Fe_5C_2, demonstrating that most of the α-Fe phases were transformed to Fe_5C_2. The low peak intensity indicated a low crystallinity of the formed Fe_5C_2 during the in-situ carburization in CO gas flow during the reaction. For the Fe/TiC catalyst with a high Fe loading of 15 w%, a slight amount of Fe_3O_4 existed in the catalysts. CoO peaks were observed in the XRD patterns in Co/TiC before the reaction. After the reaction, Co_2C was formed. The Co_2C particles were probably also the active sites for CO hydrogenation in Co/TiC.[29,30]

The X-ray photoelectron spectroscopy (XPS) survey spectrum of the Fe–Co(5:1)/TiC catalyst possessed characteristic peaks of C 1s, K 2s, Ti 2p, O 1s, Fe 2p, and Co 2p (Figure 2c). The K 2s peak was determined because we added K^+ promoters during the catalyst preparation. Under the dark conditions for the fresh and in-situ carburized Fe–Co(5:1)/TiC catalysts, the Fe 2p spectra were attributed to the Fe^{2+} state (Figure 2d). Under light irradiation, we observed a more than 1.0 eV shift of the Fe 2p spectra towards the lower binding energy, indicating that the chemical states of Fe were reduced to between 0 and

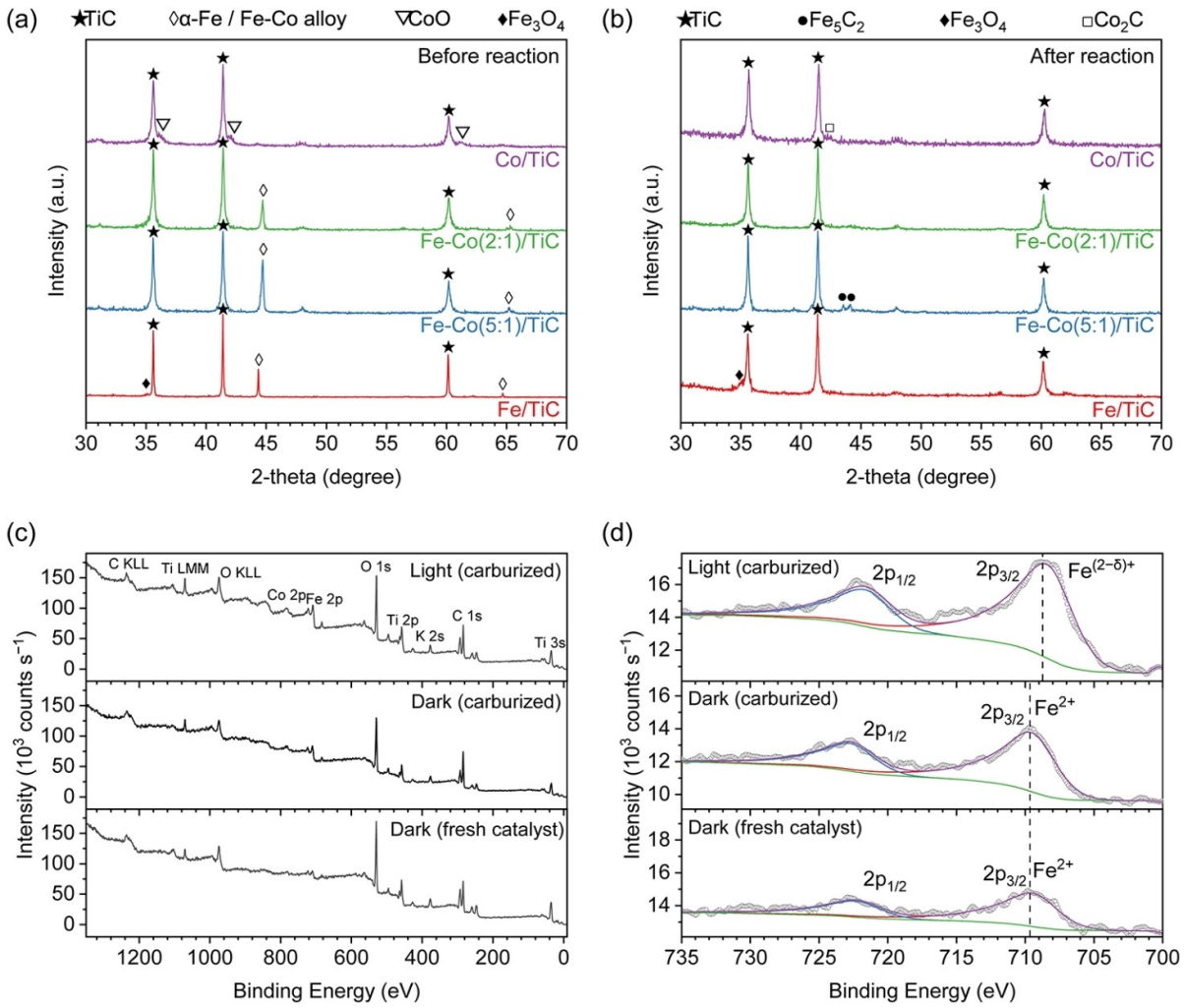

Figure 2. XRD patterns of Fe/TiC, Fe–Co/TiC, Co/TiC a) before and b) after CO hydrogenation under light irradiation. c) XPS survey spectrum and d) high-resolution scan of Fe 2p.

+2. Thus, we hypothesized that the photo-excited plasmonic hot electrons generated on TiC might transfer to Fe_5C_2 through the TiC/Fe_5C_2 interfaces, and reduce the chemical states of Fe.

The SEM images of all the catalysts before and after the reaction are shown in Figures S3 and S4. Fe- and Co-related nanoparticles were randomly located on the surfaces of TiC supports. SEM-EDX mapping of the Fe–Co(5:1)/TiC catalyst (Figure S5) showed a homogeneous distribution of Fe, Co, and K^+ elements on TiC. No obvious particle aggregation was observed after the CO hydrogenation reaction. The TEM images and STEM-EDX mapping of the used Fe–Co(5:1)/TiC catalyst are presented in Figure 3. The high-resolution TEM image in panel (b) shows the distinct lattice fringes with a d-spacing of 0.22 nm, in line with the (220) lattice planes of TiC support. In addition, the lattice fringe with a d-spacing of ~0.21 nm corresponds to the (021) facet of Fe_5C_2 (Figure S8), which agreed with the XRD peaks at 43.4° in Figure 2a. As shown in the STEM image and EDX mapping in panels (c)–(i), Co-doped Fe_5C_2 nanoparticles were located on the surfaces of TiC particles.

As shown in the photothermal performance in Figure 4a, adding Co into Fe_5C_2 catalysts increases the CO conversion under both dark (thermal) and light (photothermal) conditions. This is because Co could promote the H_2 activation to form CH_x species and increase CO hydrogenation. As shown in Figure 4c, for the Co/TiC catalysts, the increased amount of CO conversion mainly goes to CH_4 as compared to that with Fe–Co(5:1) and Fe–Co(2:1) catalysts, indicating that Fe_5C_2 is more active than CoC_2 for the multi-carbon generation. Compared to the thermal catalytic process under dark conditions, the photothermal CO conversion under light irradiation showed obvious enhancement (Figure 4b). This is likely because light irradiation increased the surface temperature to promote the reaction. Also, the generated plasmonic hot electrons on TiC might transfer to Fe_5C_2 and activate Fe_5C_2 surfaces for improved CO conversion. Figure 4c depicted the distribution details of the hydrocarbon products of different catalysts with and without light irradiation. Among the produced hydrocarbons, C_{2+} products were over 50% with Fe/TiC, Fe–Co(5:1)/TiC, and Fe–Co(2:1)/TiC under light irradiation, higher than those

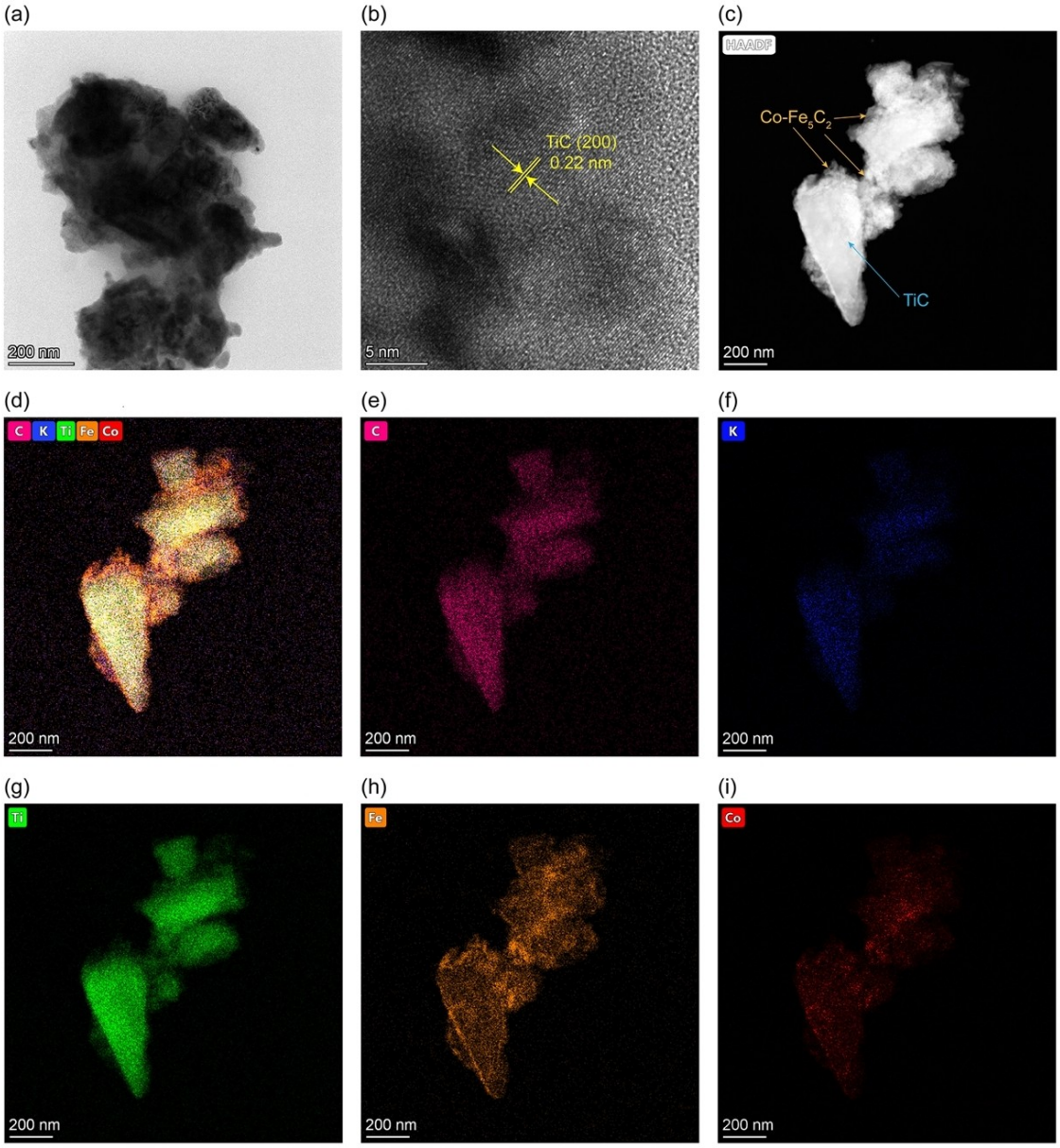

Figure 3. TEM images of Fe–Co(5:1)/TiC after the photothermal reaction: a) TEM image, b) HR-TEM image, c) HAADF-STEM image, and d)–i) STEM-EDX mapping of C, K, Ti, Fe, and Co.

obtained with Co/TiC under the same conditions. The gradual increase in CH_4 proportion with the increasing Co loading indicated that Co sites were active for CH_4 formation. In addition, the proportions of C_2–C_3 products in the Fe–Co/TiC and Co/TiC catalysts were 19–21% under dark conditions, which implied the variation of Co content had a limited effect on the distribution of C_2–C_3 products under dark conditions, but the yields of C_2–C_3 products increased with the increase of the Co content, likely because that adding Co promoted H_2 dissociation. Under irradiated conditions, Fe–Co(5:1) catalyst showed the highest C_2–C_3 proportion up to 32%. However, distinct from the other three catalysts, Co/TiC catalyst without Fe-loading tended to produce CH_4 under light irradiation conditions, resulting in a high percentage of 73% CH_4 production in the hydrocarbon products. This likely indicated that Fe_5C_2 was active for C_{2+} production, and Co was used to promote H_2 dissociation and CH_x formation. As a result, the Fe–Co/TiC catalysts showed optimal CO conversion and C_2–C_3 selectivity and yield. Fe–Co(5:1) exhibited a ~8-fold increase in CO conversion and ~7-fold increase in C_{2+} yield under irradiation.

Further, we analyzed the gaseous and liquid products using a gas chromatograph with a flame ionization detector (GC-FID) and a gas chromatography-mass spectrometry (GC-MS), respectively. As shown in Figure S9, we calculated the ASF chain growth probability (α) to be ~0.35 from the distribution of C_1–C_5 olefins and paraffins in the gaseous products. Also, the C_7–C_{20+} long-chain products of olefins, paraffins, and aromatics

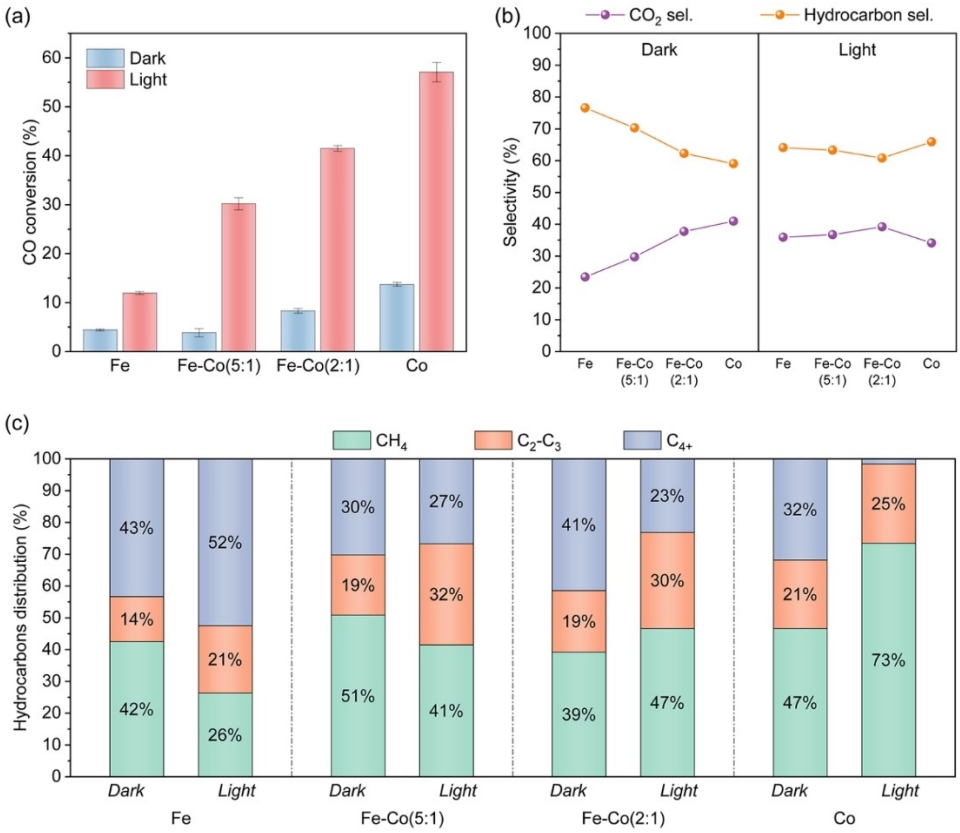

Figure 4. a) CO conversion, b) hydrocarbon and CO_2 selectivity, and c) hydrocarbon distributions of catalysts under light irradiation or direct heating. Reaction conditions: 350 °C, 0.5 Mpa, $CO/H_2/Ar = 24:72:4$, 50 mg catalyst. The error bars were calculated based on three independent experiments.

were observed in the photothermal CO hydrogenation (Table S1).

We also did a control experiment by coating a thin layer of TaC on top of the Fe–Co(5:1)/TiC catalyst (Figure S6). TaC coating prevented direct light irradiation on the Fe–Co(5:1)/TiC so that there was almost no light-induced hot-electron injection from TiC nanoparticles to Fe_5C_2 sites. TaC is a good photothermal material,[31] which enables the same surface temperature (~385 °C) on the TaC-coated catalysts as that on Fe–Co-(5:1)/TiC under irradiation. As shown in Figure S7, the CO conversion was 14% using the TaC-coated Fe–Co(5:1)/TiC under the same surface temperature and in the same reactant gas flow, half of the performance of the Fe–Co(5:1)/TiC without TaC coating. This result indicated that the plasmonic non-thermal effect, namely the hot-electron injection from TiC to Fe_5C_2, could contribute to the reaction and increase the CO conversion and C_2–C_3 selectivity.

Conclusion

In summary, photothermal Co–Fe_5C_2/TiC catalysts were prepared by wet impregnation and in-situ carburization. In-situ-irradiated XPS indicated that hot electron injection from TiC to Fe_5C_2 through the TiC/Fe_5C_2 interfaces reduced the chemical states of Fe to promote the photothermal CO hydrogenation. The C_{2+} selectivity increased to 59%, the C_2–C_3 selectivity increased to 32%, and the CO conversion increased to >30% under photothermal catalytic conditions. These results are important for understanding the mechanism of plasmonic-promoted catalytic activity as well as for developing new photothermal catalysts by coupling the catalytic and plasmonic units for improved C–C bond formation and CO hydrogenation.

Experimental Section

Catalyst preparation: Titanium carbide (TiC), basic iron(III) acetate ($FeOH(Ac)_2 \cdot nH_2O$), and cobalt acetate ($Co(Ac)_2 \cdot 4H_2O$) were purchased from Macklin Co. Ltd. They were used without further purification. Powder catalysts were synthesized according to a wet impregnation method. In brief, 500 mg TiC powder was immersed into a mixed aqueous solution containing different amounts of $FeOH(Ac)_2$ and $Co(Ac)_2$. The obtained power was dried overnight at 120 °C and calcinated in the mixed gas of $H_2/Ar = 5:95$ at 500 °C for 4 h. Then the obtained powder was added to the K_2CO_3 aqueous solution and repeated the steps of drying and calcination to load potassium ions onto the catalysts. Four catalysts with the same K and TiC contents (5 wt% K and 500 mg TiC) and different Fe and Co concentrations, including 15 wt% Fe (Cat. Fe/TiC), 12.5 wt% Fe mixed with 2.5 wt% Co (Cat. Fe–Co(5:1)/TiC), 10 wt% Fe mixed with 5 wt% Co (Cat. Fe–Co/TiC) and 15 wt% Co (Cat. Co /TiC), were prepared.

Characterization: X-ray diffraction (Bruker Advantage D8 diffractometer with $Cu_{K\alpha}$ radiation and a D/teX Ultra detector), SEM (Hitachi Regulus SU8100 instrument with an EDS analyzer), TEM (and/or STEM, FEI TALOS F200X at an accelerating voltage of 200 kV), UV-vis-NIR (Shimadzu UV3600Plus spectrometer with a diffuse reflection unit), and XPS (Thermo Scientific ESCALAB 250Xi Spectrometer) were conducted to characterize the catalysts.

Performance evaluation. The prepared powder catalysts were placed into a flow reactor. 50 mg catalyst was filled into the built-in stainless sample cup in the reactor (Harrick MRA-5) and pre-activated in pure CO for 1 h at 400 °C and ambient pressures. The catalyst performance tests were carried out in the reactant gas of $CO/H_2/Ar = 24:72:4$ at 350 °C and 0.5 Mpa for both the dark and irradiated conditions. A 300 W Xe lamp (CME-303, Microenerg Beijing Technology, equipped with a quartz guidance fiber) was used as the light source to implement light irradiation. We used an optical power meter (CEL-NP2000-10A, CEAulight) to measure the light intensity at the same working distance of ~1 cm from the optical guidance fiber to the catalyst surface used in the photothermal catalytic reaction. The light intensity is ~1.6 W. The surface temperature was measured by an infrared irradiation meter (SA-D5050A, Wuxi Shiao) under light irradiation. Agilent 990 micro-gas chromatograph (μGC) equipped with micro-thermal conductivity detectors (μTCD) was used for online tests to detect the CO hydrogenation products. The gaseous and liquid products were analyzed by a gas chromatograph with a flame ionization detector (GC-FID, GC-9860-5C-NJ, Nanjing Hope Analytical equipment Co. Ltd.) and a gas chromatography-mass spectrometry (GC-MS, GC2010, Shimadzu).

Acknowledgements

This work was supported by the National Key Research and Development Program of the Ministry of Science and Technology of China (no. 2020YFA0406102), the National Natural Science Foundation of China (grant no. 22272078, 91963121), and the Frontiers Science Center for Critical Earth Material Cycling of Nanjing University.

Conflict of Interest

The authors declare no conflict of interest.

Data Availability Statement

The data that support the findings of this study are available from the corresponding author upon reasonable request.

Keywords: CO hydrogenation · C_{2+} hydrocarbons · metal carbides · photothermal catalyst · surface plasmon resonance

[1] P. Zhai, G. Sun, Q. Zhu, D. Ma, *Nanotechnol. Rev.* **2013**, *2*, 547–576.
[2] K. Cheng, W. Zhou, J. Kang, S. He, S. Shi, Q. Zhang, Y. Pan, W. Wen, Y. Wang, *Chem* **2017**, *3*, 334–347.
[3] N. Keller, J. Ivanez, J. Highfield, A. M. Ruppert, *Appl. Catal. B* **2021**, *296*, 120320.
[4] S. Du, X. Bian, Y. Zhao, R. Shi, T. Zhang, *Chem. Res. Chin. Univ.* **2022**, *38*, 723–734.
[5] G. Chen, G. I. N. Waterhouse, R. Shi, J. Zhao, Z. Li, L. Wu, C. Tung, T. Zhang, *Angew. Chem. Int. Ed.* **2019**, *58*, 17528–17551; *Angew. Chem.* **2019**, *131*, 17690–17715.
[6] H. Lyu, B. Hu, G. Liu, X. Hong, L. Zhuang, **n.d.**, 9.
[7] C. Qiu, S. Bai, W. Cao, L. Tan, J. Liu, Y. Zhao, Y.-F. Song, *Trans. Tianjin Univ.* **2020**, *26*, 352–361.
[8] H. L. Huynh, W. M. Tucho, Z. Yu, *Green Energy & Environ.* **2020**, *5*, 423–432.
[9] H. Liu, H. Ye, M. Gao, Q. Li, Z. Liu, A. Xie, L. Zhu, G. W. Ho, S. Chen, *Adv. Sci.* **2021**, *8*, 2101232.
[10] M. Zhong, K. Tran, Y. Min, C. Wang, Z. Wang, C.-T. Dinh, P. De Luna, Z. Yu, A. S. Rasouli, P. Brodersen, S. Sun, O. Voznyy, C.-S. Tan, M. Askerka, F. Che, M. Liu, A. Seifitokaldani, Y. Pang, S.-C. Lo, A. Ip, Z. Ulissi, E. H. Sargent, *Nature* **2020**, *581*, 178–183.
[11] L. Li, A. Ozden, S. Guo, F. P. García de Arquer, C. Wang, M. Zhang, J. Zhang, H. Jiang, W. Wang, H. Dong, D. Sinton, E. H. Sargent, M. Zhong, *Nat. Commun.* **2021**, *12*, 5223.
[12] S. Shoji, X. Peng, A. Yamaguchi, R. Watanabe, C. Fukuhara, Y. Cho, T. Yamamoto, S. Matsumura, M.-W. Yu, S. Ishii, T. Fujita, H. Abe, M. Miyauchi, *Nat. Catal.* **2020**, *3*, 148–153.
[13] H. Robatjazi, H. Zhao, D. F. Swearer, N. J. Hogan, L. Zhou, A. Alabastri, M. J. McClain, P. Nordlander, N. J. Halas, *Nat. Commun.* **2017**, *8*, 1–10.
[14] X. Zhang, X. Li, D. Zhang, N. Q. Su, W. Yang, H. O. Everitt, J. Liu, *Nat. Commun.* **2017**, *8*, 14542.
[15] J. Wei, F. L. Meng, T. Li, T. Zhang, S. Xi, W. L. Ong, X. Wang, X. Zhang, M. Bosman, G. W. Ho, *Adv. Funct. Mater.* **2022**, *32*, 2109693.
[16] Y. Wang, J. Zhang, W. Liang, H. Yang, T. Guan, B. Zhao, Y. Sun, L. Chi, L. Jiang, *CCS* **2022**, *4*, 1153–1168.
[17] X.-N. Guo, Z.-F. Jiao, G.-Q. Jin, X.-Y. Guo, *ACS Catal.* **2015**, *5*, 3836–3840.
[18] Y. Wang, Y. Zhao, J. Liu, Z. Li, G. I. N. Waterhouse, R. Shi, X. Wen, T. Zhang, *Adv. Energy Mater.* **2020**, *10*, 1902860.
[19] K. Feng, S. Wang, D. Zhang, L. Wang, Y. Yu, K. Feng, Z. Li, Z. Zhu, C. Li, M. Cai, Z. Wu, N. Kong, B. Yan, J. Zhong, X. Zhang, G. A. Ozin, L. He, *Adv. Mater.* **2020**, *32*, 2000014.
[20] H. Zhao, J.-X. Liu, C. Yang, S. Yao, H.-Y. Su, Z. Gao, M. Dong, J. Wang, A. I. Rykov, J. Wang, Y. Hou, W.-X. Li, D. Ma, *CCS* **2020**, *3*, 2712–2724.
[21] Z. Li, J. Liu, Y. Zhao, R. Shi, G. I. N. Waterhouse, Y. Wang, L.-Z. Wu, C.-H. Tung, T. Zhang, *Nano Energy* **2019**, *60*, 467–475.
[22] C. Yang, H. Zhao, Y. Hou, D. Ma, *J. Am. Chem. Soc.* **2012**, *134*, 15814–15821.
[23] S. Lögdberg, D. Tristantini, Ø. Borg, L. Ilver, B. Gevert, S. Järås, E. A. Blekkan, A. Holmen, *Appl. Catal. B* **2009**, *89*, 167–182.
[24] M. C. Soydan, A. Ghobadi, D. U. Yildirim, V. B. Erturk, E. Ozbay, *Plasmonics* **2019**, *14*, 1801–1815.
[25] S. Ishii, S. L. Shinde, T. Nagao, *Adv. Opt. Mater.* **2019**, *7*, 1800603.
[26] H. Bai, W. Liu, W. Yi, X. Li, J. Zhai, J. Li, J. Liu, H. Yang, G. Xi, *Chem. Commun.* **2018**, *54*, 10843–10846.
[27] M. Kumar, N. Umezawa, S. Ishii, T. Nagao, *ACS Photonics* **2016**, *3*, 43–50.
[28] J. Chai, R. Pestman, W. Chen, A. I. Dugulan, B. Feng, Z. Men, P. Wang, E. J. M. Hensen, *J. Catal.* **2021**, *400*, 93–102.
[29] J. C. Mohandas, M. K. Gnanamani, G. Jacobs, W. Ma, Y. Ji, S. Khalid, B. H. Davis, *ACS Catal.* **2011**, *1*, 1581–1588.
[30] L. Zhong, F. Yu, Y. An, Y. Zhao, Y. Sun, Z. Li, T. Lin, Y. Lin, X. Qi, Y. Dai, L. Gu, J. Hu, S. Jin, Q. Shen, H. Wang, *Nature* **2016**, *538*, 84–87.
[31] O. Anjaneyulu, K. Takeda, S. Ishii, S. Ueda, T. Nagao, P. Xiaobo, T. Fujita, M. Miyauchi, H. Abe, *Mater. Chem. Front.* **2018**, *2*, 580–584.

Manuscript received: September 15, 2022
Accepted manuscript online: November 21, 2022
Version of record online: January 3, 2023